54
10-2-74
Special ENDF Distr.

ORNL-TM-4222

(ENDF 188)

SDT 11. THE ORNL BENCHMARK EXPERIMENT FOR NEUTRON TRANSPORT THROUGH IRON AND STAINLESS STEEL, PART I

R. E. Maerker

MASTER

OAK RIDGE NATIONAL LABORATORY

OPERATED BY UNION CARBIDE CORPORATION • FOR THE U.S. ATOMIC ENERGY COMMISSION

DISCLAIMER

ORNL-TM-4222
(ENDF 188)

Contract No. W-7405-Eng-26

Neutron Physics Division

SDT11. THE ORNL BENCHMARK EXPERIMENT FOR NEUTRON TRANSPORT THROUGH IRON AND STAINLESS STEEL, PART I

R. E. Maerker

Reference: R. E. Maerker and F. J. Muckenthaler, "Final Report on a Benchmark Experiment for Neutron Transport Through Iron and Stainless Steel," ORNL-4892 (1974)

SEPTEMBER 1974

OAK RIDGE NATIONAL LABORATORY
Oak Ridge, Tennessee 37830
operated by
UNION CARBIDE CORPORATION
for the
U. S. ATOMIC ENERGY COMMISSION

THIS PAGE

WAS INTENTIONALLY

LEFT BLANK

TABLE OF CONTENTS

THIS PAGE

WAS INTENTIONALLY

LEFT BLANK

ABSTRACT

The first part of an experiment concerning deep neutron penetration in iron and stainless steel is described, and experimental results in a format for CSEWG shielding integral data testing are presented. These results provide a basis for verification of the accuracy of iron and stainless steel cross sections used in transport calculations. The experiment was performed at the Tower Shielding Facility of ORNL and included measurements of both the neutron fluence and neutron spectra behind slabs of iron up to 3 ft thick and of stainless steel up to 1 ft thick.

DESCRIPTION OF THE EXPERIMENT AND SOURCE DATA

Both the top shield and the structural components in the design of a fast reactor, and the thermal shield of a conventional thermal reactor contain a large amount of iron in the form of carbon and stainless steels, and iron therefore constitutes an important part of the neutron shield. The carbon steels consist of relatively pure (i.e., 98-99%) iron, while the stainless steels contain, in addition to about 70% iron, considerable amounts of chromium and nickel. Since these steel components have thicknesses of the order of 3 ft, it is essential that accurate experimental results be available to verify transport calculations for deep penetration of neutrons through iron and stainless steel.

Consequently, a series of transmission measurements of neutrons above thermal energies through various thicknesses of iron slabs and also through a 12-in. stainless steel slab have been performed at the Tower Shielding Facility using a collimated beam of reactor neutrons as a source. These measurements were made behind various combinations of thin (i.e., ½ to 2 in. thick) 5 ft by 5 ft slabs; measurements were obtained behind iron thicknesses of approximately 1.5, 4, 6, 12, 24, and 36 in. Figure 1 shows a schematic of the experimental geometry for the 36-in. case.

The thickness, density, and composition of the individual slabs used in the experiment were accurately determined. The density of the type 304 stainless steel slabs averaged 7.86 g/cm^3 and the density of the iron slabs averaged 7.79 g/cm^3. The composition of the slabs is shown in Table I, where it is to be observed that the "iron" slabs were actually carbon (i.e., mild) steel.

Sufficient measurements of the incident neutron beam were made that an absolute energy spectrum from thermal to 10 MeV could be obtained for use in calculations. This incident spectrum is presented in Table II in a 220-group structure. The intensities in Table II are for any point on the exit plane of the collimator located within a diameter of 6½ in. Mapping of the incident beam along the axial direction established the

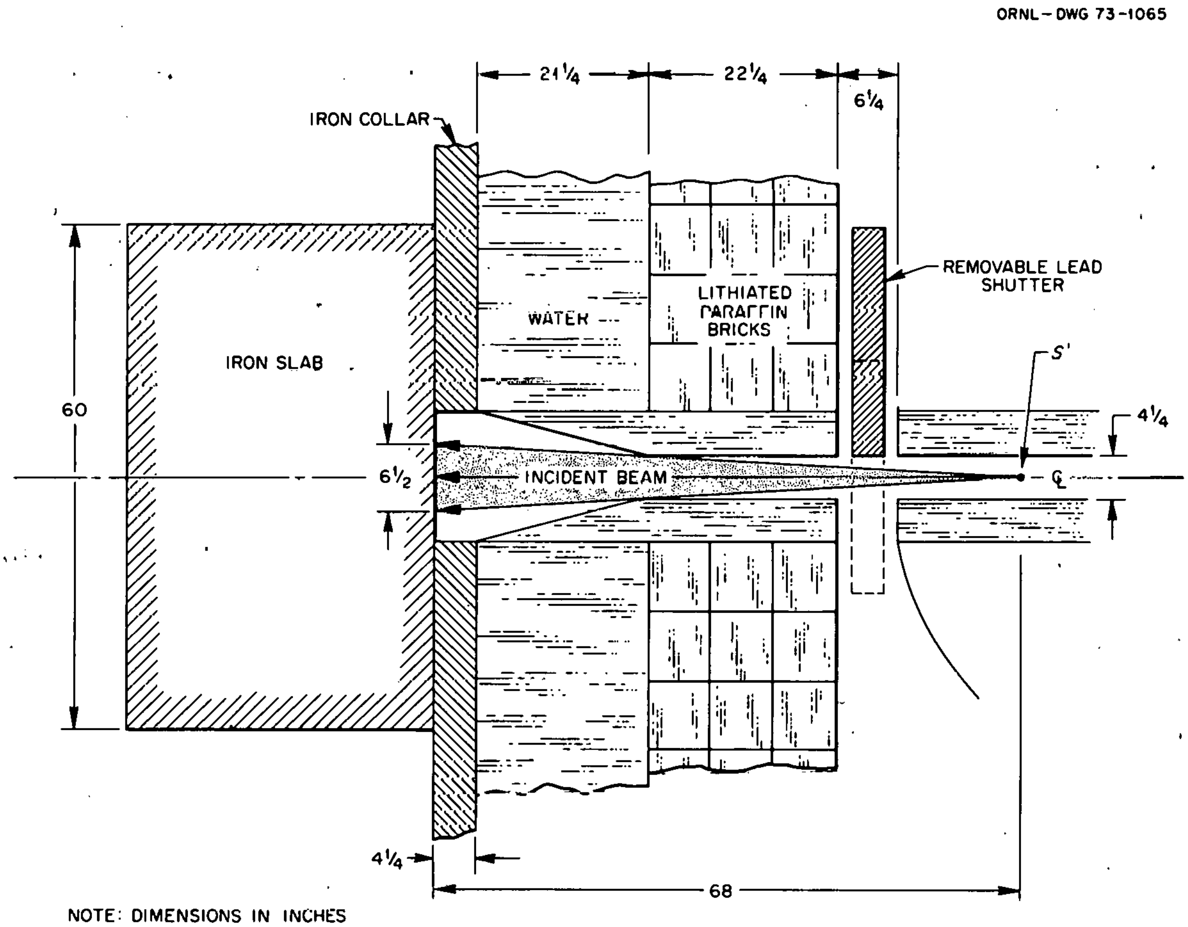

Fig. 1. Experimental Configuration for the 4-1/4-in.-diam Collimator with the 3-ft-Thick Iron Slab in Place. (This collimator was used for all the measurements except those made behind 18 in. of stainless steel.)

fact that the tightly collimated source could be represented as a virtual point anisotropic source located 68 in. inside the collimator from the edge of the iron collar (point S' in Fig. 1) with the beam intensity uniform over a diameter of 6½ in. at the mouth of the collimator and zero elsewhere. The accuracy of the incident absolute spectrum in Table I-I is estimated to be $\pm$10% down to 200 keV and $\pm$20% below 200 keV. The ratio of surface-integrated current over the collimator to centerline current is 212.5 cm^2.

Neutron spectrum measurements beyond the iron or stainless steel slabs were taken using two types of spectrometers. These were: (I) an NE-213 liquid scintillator, which determines spectra in the energy range 0.8 to 10 MeV with the aid of the unfolding code FERDOR; and (II) a Benjamin proton recoil spectrometer which determines spectra in the energy range $\sim$100 keV to 1.5 MeV with the aid of the unfolding code SPEC4. Table III gives the resolution of the NE-213 as a function of energy. The resolution of the Benjamin spectrometer is constant at 10% FWHM. In addition, a set of spherical BF_3 detectors surrounded by various thicknesses of polyethylene (0 to 5 in.) and an outside shell of cadmium were used to obtain weighted integral flux measurements. These Bonner ball detectors have response functions which peak in different regions of the spectrum. The composition of each Bonner ball and the location of the center of detection is listed in Table IV. The response function for each of the three Bonner balls in a 100 group GAM-II structure is presented in Tables V through VII. They are expressed in units of counts/sec per neutron/cm^2/sec uniformly incident over the outside hemispherical surface of the ball, and were obtained by adjoint ANISN calculations normalized to calibration experiments performed at the Tower Shielding Facility. The estimated accuracy of the response functions is also indicated in each of the tables.

DATA OBTAINED BEHIND THE SLABS

All of the measurements made behind the slabs are summarized in Tables VIII and IX. The Bonner ball data obtained from these measurements are presented in Tables X through XIV. Counting times and operating reactor powers for the Bonner ball measurements were sufficiently large that statistical errors in the Bonner ball counting rates may be assumed to be negligible. The reproducibility of all measurements lies within ±5% and is due primarily to uncertainties in the power calibration procedure. Backgrounds were obtained for each of the Bonner ball measurements by placing a hydrogenous slab midway between the rear face of the slabs and the detector. The data appearing in Tables X through XIV have been corrected for these backgrounds. Because of the underestimation of the backgrounds in the measurement procedure described above, the data in Tables X through XIV are accurate to about 10%, including uncertainties in the power calibration.

The unfolded Benjamin proton recoil spectrometer data are presented in Tables XV through XVIII, where the standard error is due to counting statistics only. The absolute energy calibration is accurate to within an estimated ±5%. No backgrounds were obtained for the Benjamin counter measurements because they were less than 5% of the measured foregrounds.

In the region of overlap between the various Benjamin counters, no particular counter should be better than the other, and the discrepancy in the two measurements is an indication of the accuracy of the Benjamin counter system.

The unfolded NE-213 liquid scintillator spectral data are presented in Tables XIX through XXIV, where the upper and lower limits of each unfolded spectrum are due to combined statistical and unfolding uncertainties. Backgrounds were obtained for each of the NE-213 measurements and the data in Tables XIX through XXIV are the results of the measurements after these backgrounds have been subtracted.

METHODS OF CALCULATION

The collimator geometry should be included in the calculations for all slab thicknesses, in order to take into account the effect of multiple reflection between the slab and the collimator, including the iron collar, on the fluxes transmitted through the slab. Referring to Fig. 1, the composition of the iron collar may be assumed to be the same as that of the iron slabs presented in Table I. Besides the water, the only remaining collimator material that needs to be considered is a ¼-in. thickness of aluminum that contains the water that was inserted into the 14-7/8-in. diam collimator. The geometry from the location of the lead shutter inward to the reactor in Fig. 1 may be ignored. The collimator is thus of cylindrical geometry and the 5 ft by 5 ft slabs may be assumed cylinders of $\sqrt{100/\pi}$ = 5.64 ft diameter with negligible error. Thus the calculations may be made using two-dimensional r,z geometry.

The calculations are best done by Monte Carlo techniques employing "point" cross sections. If groups are employed instead, a sufficient number must be used to include the most important features of the total cross-section structure in iron, which for the ORNL calculations amounted to the 220-group structure appearing in Table II. The cross sections are to be weighted within a group by $1/E\Sigma_T$. Using the multigroup Monte Carlo method, the calculations for each slab thickness can be broken up into three parts. The first calculation replaces the collimator by a vacuum and uses as the source the absolute spectrum appearing in Table II multiplied by 212.5 cm^2. The source point is sampled spatially on the exit plane of the collimator over a distance of 6.5 in. by first choosing an incident direction and then calculating the intersection of the ray with the exit plane of the collimator. Uncollided contributions to detectors located along the centerline should be calculated analytically using "point" cross sections in a separate computation using

$$\phi_{unc}(Z,E_g) = \phi_o(E_g) \times (68/68+Z)^2 \int_{E_{g\ell}}^{E_{gu}} \exp(-\Sigma_T[E]T)\, dE \Big/ (E_{gu}-E_{g\ell}) \quad , \quad (1)$$

where the $\Sigma_T(E)$ are "point" values in cm^{-1}, the $\phi_o(E_g)$ are taken directly from Table II, E_{gu} and $E_{g\ell}$ are the upper and lower limits of the group E_g, T is the thickness of the slab in cm, and Z is the distance from the detector to the open end of the collimator, in inches. The second calculation includes the collimator and uses the same source as before, but

but uses a coarser group structure to calculate the absolute spectral and spatial distribution of the multiply reflected current incident upon the slab over the entire exit plane of the collimator, including the iron collar. The third calculation uses the absolute source computed in the second calculation, with simplifying assumptions regarding the re-incident angular distribution (i.e., cosine) and spectrum, to calculate the transmitted fluxes through the slabs arising from the re-incident neutrons again using a 220-group structure. The second calculation quickly saturates with increasing slab thickness, and need not be done every time. However, the first and third calculations should be performed for every slab thickness. Biasing in the first and third steps of the calculation is optional (path length stretching of the order of a factor of two through the 24-in. and 36-in. slabs), and is not at all necessary in the second step.

The approximate contribution of the multiple-reflected collimator fluxes in this experiment is shown in Table XXV, where the calculated ratios of the transmitted fluxes above thermal energy that arise as a result of scattering in the slabs including the first, second, and third steps in the calculation to only the first step of the calculation are shown.

The effect of the group structure on the transmitted spectral fluxes is shown in Table XXVI, where the results of two ANISN calculations are presented for the number of neutrons in various energy groups leaking a 1 meter radius "iron" (composition given in Table I) sphere per source fission neutron located at the center. Both cross-section sets were weighted $1/E\sigma_{T_{Fe}}'$.

From Table XXVI, it is obvious that the 220-group structure, which is tailored to the minima in the total cross section, in general produces higher fluxes leaking the sphere than the standard 100 GAM-II group structure. Hence, using such a tailored set is recommended if the ENDF/B evaluation is to be tested, with at least a P_3 expansion in the angular distribution of scattering.

Calculations of this experiment may also use the discrete ordinates technique. The collimator geometry should be included, and the virtual point anisotropic source description used. Thus the source has an intensity of $4\pi(68 \times 2.54)^2 = 3.75 \times 10^5$ times the entries in Table II in neutrons/min/watt, at a point 68 in. inside the collimator, constant over the solid angle $1 \leq \cos\theta \leq 0.99887$, $0 \leq \phi \leq 2\pi$, and zero elsewhere. A first collision source routine in the two-dimensional discrete ordinates calculation is recommended for the centerline detector locations, else the uncollided contribution is incorrectly calculated and difficult to extract. The uncollided contribution is calculated in a separate computation completely identical to the calculation described earlier following the Monte Carlo discussion.

A routine is also necessary to calculate the slab scattered fluxes at the detector locations from discrete ordinate calculated fluxes in the slabs. This is done by such codes as SPACETRAN or FALSTF that are available at ORNL. The use of DOT-III, an updated version of the DOT two-dimensional discrete ordinates code, is to be used, since it incorporates the first collision source and provides a tape suitable for FALSTF. The fluxes are very sensitive to the detector location, especially in the vicinity of the rear face of the slab, and the routine SPACETRAN or FALSTF should always be used.

No thermal-neutron calculations are necessary for this experiment since the detectors used have zero sensitivity to thermal neutrons.

Calculations of the NE-213 and Benjamin counter spectra should be smoothed with the resolution function of the spectrometer before comparing with experimental data. Air attenuation from the rear face of the slabs to the detectors is to be neglected, since it was also neglected in the derivation of the source terms. Calculation of the Bonner ball counting rates involve evaluation of the following expression:

$$\text{Counts/min/watt}(r) = \sum_g \phi(E_g, r-\Delta)\, R(E_g) \quad , \tag{2}$$

where

r is the distance of the geometric center of the ball from the center of the exit face of the slabs,

Δ is the center of detection correction given in Table IV,

$r-\Delta$ is the location of the detector for the calculated fluxes,

$R(E_g)$ is the interpolated response function of the Bonner ball for group E_g.

Note that the numbering of the groups in the response function tabulation in Tables V-VII has been reversed so that $R(E_g)$ in Eq. (2) appears as $R(E_{101-g})$ in the tables. Neglect of Δ in Eq. (2) can lead to underestimates of the order of 5% in the calculated counting rates, the error being the greatest for the 10 in. Bonner ball at the closest location behind the slabs.

Table I. Composition of the Slabs in Atoms/barn-cm

	Iron Slabs	Stainless Steel Slabs
Carbon	9.815(-4)[a]	-
Manganese	5.15(-4)	1.14(-3)
Iron	8.372(-2)	5.995(-2)
Chromium	-	1.686(-2)
Nickel	-	7.90(-3)

[a]Read: 9.815×10^{-4}.

Table II. Source Spectrum at the End of the Collimator in neuts/cm^2/min/watt/group*

Group	Energy Interval	Intensity	Group	Energy Interval	Intensity
1	8-10 MeV	190	31	1.405-1.411 MeV	23.8
2	6-8	665	32	1.401-1.405	16.6
3	5-6	840	33	1.392-1.401	35.4
4	4-5	1426	34	1.382-1.392	40.1
5	3-4	2186	35	1.363-1.382	74.5
6	2.59-3	1479	36	1.339-1.363	93.5
7	2.38-2.59	887	37	1.313-1.339	98.2
8	2.35-2.38	130	38	1.306-1.313	25.9
9	2.262-2.35	384	39	1.291-1.306	56.8
10	2.232-2.262	130	40	1.285-1.291	22.5
11	1.943-2.232	1267	41	1.251-1.285	125
12	1.90-1.943	190	42	1.244-1.251	25.9
13	1.889-1.90	47.5	43	1.221-1.244	84.5
14	1.82-1.889	301	44	1.217-1.221	14.2
15	1.81-1.82	43.8	45	1.211-1.217	21.3
16	1.783-1.81	118	46	1.205-1.211	21.2
17	1.747-1.783	153	47	1.197-1.205	28.4
18	1.722-1.747	109	48	1.192-1.197	17.7
19	1.686-1.722	153	49	1.169-1.192	79.2
20	1.680-1.686	25.9	50	1.155-1.169	48.6
21	1.6465-1.680	143	51	1.136-1.155	65.0
22	1.638-1.6465	39.1	52	1.130-1.136	20.1
23	1.587-1.638	219	53	1.1195-1.130	34.3
24	1.567-1.587	85.0	54	1.1165-1.1195	10.0
25	1.522-1.567	190	55	1.1135-1.1165	10.0
26	1.506-1.522	67.6	56	1.107-1.1135	23.8
27	1.497-1.506	38.0	57	1.098-1.107	29.6
28	1.472-1.497	104	58	1.090-1.098	26.0
29	1.442-1.472	125	59	1.084-1.090	20.1
30	1.411-1.442	124	60	1.029-1.084	177

Table II (Cont'd.)

Group	Energy Interval	Intensity	Group	Energy Interval	Intensity
61	1.023-1.029 MeV	20.1	91	825-830 keV	20.1
62	1.020-1.023	10.0	92	820-825	20.6
63	1.013-1.020	23.8	93	769-820	216
64	0.998-1.013	49.6	94	767-769	8.98
65	992-998 keV	19.5	95	752.5-767	67.6
66	982-992	32.8	96	751-752.5	6.85
67	974-982	26.4	97	741-751	47.5
68	960-974	46.5	98	739-741	9.49
69	957-960	10.0	99	732-739	33.8
70	951-957	20.1	100	710-732	107
71	946-951	16.9	101	700-710	48.6
72	944-946	6.85	102	697-700	14.8
73	941.5-944	8.44	103	693-697	19.5
74	939.5-941.5	6.85	104	691-693	9.49
75	936-939.5	12.1	105	663-691	134
76	932-936	13.7	106	659-663	19.0
77	927-932	17.4	107	652.5-659	30.6
78	919-927	28.0	108	648-652.5	21.1
79	917-919	7.39	109	644-648	18.5
80	898.5-917	65.5	110	638-644	28.0
81	891-898.5	27.5	111	620-638	82.9
82	882-891	33.3	112	616.5-620	15.8
83	878-882	14.8	113	612.5-616.5	18.0
84	855.5-878	85.5	114	607.5-612.5	22.2
85	852.5-855.5	11.6	115	590.5-607.5	75.5
86	846.5-852.5	23.2	116	580-590.5	45.9
87	839-846.5	29.6	117	576-580	16.9
88	836-839	12.1	118	569.6-576	27.5
89	834-836	7.93	119	560.5-569.5	38.0
90	830-834	15.8	120	559-560.5	6.34

Table II (Cont'd.)

Group	Energy Interval	Intensity	Group	Energy Interval	Intensity
121	557.5-559 keV	6.34	151	330.7-331.4 keV	3.66
122	552.5-557.5	21.1	152	314-330.7	87.3
123	546.5-552.5	24.8	153	309.5-314	23.7
124	543-546.5	14.2	154	300-309.5	50.2
125	540-543	12.7	155	275-300	135
126	536-540	16.4	156	271-275	21.9
127	534-536	8.12	157	267-271	21.9
128	515-534	77.1	158	262-267	27.5
129	510.5-515	18.0	159	244.8-262	94.7
130	503-510.5	29.6	160	244-244.8	4.41
131	498-503	19.5	161	243.2-244	4.41
132	493-498	19.0	162	232-243.2	61.8
133	469.1-493	90.6	163	219.8-232	65.5
134	467.5-469.1	5.99	164	218.6-219.8	6.34
135	464-467.5	13.2	165	208-218.6	56.0
136	437.7-464	99.2	166	200=208	42.2
137	436.5-437.7	4.52	167	185.2-200	78.2
128	433-436.5	13.5	168	182-185.2	16.8
139	378-433	229	169	175-182	36.4
140	377.2-378	3.73	170	168.5-175	34.5
141	375-377.2	10.2	171	167.5-168.5	5.38
142	373.5-375	6.98	172	164-167.5	18.9
143	359.3-373.5	68.3	173	155-164	49.6
144	358.8-359.3	2.42	174	144-155	63.9
145	357.8-358.8	4.81	175	139.5-144	27.4
146	357.5-357.8	2.39	176	138.3-139.5	7.45
147	354.5-357.3	13.8	177	136.2-138.3	13.3
148	250.5-354.5	20.1	178	134-136.2	14.0
149	348.2-350.5	11.5	179	130-134	26.1
150	331.4-348.2	85.4	180	129.2-130	5.29

Table II (Cont'd.)

Group	Energy Interval	Intensity	Group	Energy Interval	Intensity
181	127.5-129.2 keV	11.3	203	15-19 keV	158
182	110-127.5	127	204	10-15	264
183	87-110	193	205	8.8-10	81.3
184	83-87	37.1	206	8.2-8.8	44.3
185	82.7-83	2.85	207	6.7-8.2	126
186	82.4-82.7	2.85	208	5.8-6.7	87.6
187	81.4-82.4	9.49	209	4.3-5.8	174
188	80-81.4	13.3	210	3.7-4.3	86.6
189	77-80	29.2	211	1.16-3.7	640
190	72-77	51.0	212	1.14-1.16	8.98
191	68-72	44.1	213	0.3167-1.14	616
192	62-68	72.4	214	88-316.7 eV	565
193	38-62	354	215	24.4-88	554
194	31-38	143	216	6.79-24.4	554
195	27-31	97.4	217	1.89-6.79	555
196	25.7-27	34.3	218	0.524-1.89	576
197	25.2-25.7	13.7	219	0.145-0.524	1542
198	24.5-25.2	19.9	220	0-0.145	6580
199	23.75-24.5	21.5	Totals, 1-220	0-10 MeV	3.186×10^4
200	23.25-23.75	14.8			
201	22-23.25	38.3			
202	19-22	100			

*For other group structures, interpolation in this table should follow the rule that Intensity/$\ell n[E_u/E_\ell]$ is constant within the interval $\Delta E = E_u - E_\ell$, where ΔE is the tabulated energy interval.

Table III. Energy Resolution of the NE-213 Spectrometer System†

E (MeV)	a(E) FWHM (%)	E (MeV)	a(E) FWHM (%)	E (MeV)	a(E) FWHM (%)
0.5	47.5	3.5	18.2	7.0	12.6
0.6	44	3.6	18.0	7.2	12.4
0.7	41	3.7	17.7	7.4	12.2
0.8	38.5	3.8	17.4	7.6	12.1
0.9	36	3.9	17.1	7.8	11.9
1.0	33.5	4.0	16.9	8.0	11.8
1.1	32.5	4.1	16.7	8.2	11.6
1.2	31	4.2	16.5	8.4	11.5
1.3	30	4.3	16.3	8.6	11.4
1.4	29	4.4	16.1	8.8	11.3
1.5	27.5	4.5	15.9	9.0	11.2
1.6	26.5	4.6	15.7	9.2	11.1
1.7	26	4.7	15.5	9.4	10.9
1.8	25	4.8	15.3	9.6	10.8
1.9	24.5	4.9	15.2	9.8	10.7
2.0	24	5.0	15.1	10.0	10.5
2.1	23.5	5.1	14.9	10.2	10.3
2.2	23	5.2	14.7	10.4	10.2
2.3	22.5	5.3	14.5	10.6	10.1
2.4	22	5.4	14.4	10.8	10.0
2.5	21.5	5.5	14.3	11.0	9.8
2.6	21.2	5.6	14.2	11.4	9.7
2.7	20.8	5.7	14.1	11.8	9.6
2.8	20.4	5.8	13.9	12.2	9.6
2.9	20.1	5.9	13.8		
3.0	19.7	6.0	13.7		
3.1	19.4	6.2	13.5		
3.2	19.1	6.4	13.2		
3.3	18.8	6.6	13.0		
3.4	18.5	6.8	12.8		

†Interpolation in this table should follow the formula

$$a(E) = \frac{E_2 - E}{E_2 - E_1} a(E_1) + \frac{E - E_1}{E_2 - E_1} a(E_2) \ , \quad \text{where } E_1 \le E \le E_2 \ .$$

Table IV. Bonner Ball Description

Spherical, 2-in.-diam $^{10}BF_3$ Proportional Counter Surrounded by Polyethylene and 0.030 in. Cadmium

Standard Bonner Ball Designation (in.)	Polyethylene Thickness (in.)	Polyethylene Density (grams/cm^3)	Diameter of Ball (in.)	Location of Center of Detection from Center of Ball[a] (in.)
3	0.515	0.951	3.09	0.9
6	1.91	0.925	5.88	1.8
10	3.90	0.951	9.86	3.0

[a]The center of detection is displaced toward the center of gravity of the hemispherical surface upon which the neutrons are incident.

Table V. Response for 3.09 Inch Diameter Bonner Sphere*

Group No.	Midpoint Energy (eV)	Response † (counts/incident neut/cm^2)
1	Thermal	Negligible
2	4.73(-1)	4.81(-1)
3	6.07(-1)	8.03(-1)
4	7.79(-1)	9.95(-1)
5	1.00(0)	1.11(0)
6	1.29(0)	1.17(0)
7	1.65(0)	1.19(0)
8	2.12(0)	1.19(0)
9	2.72(0)	1.18(0)
10	3.49(0)	1.16(0)
11	4.49(0)	1.14(0)
12	5.76(0)	1.11(0)
13	7.40(0)	1.08(0)
14	9.50(0)	1.05(0)
15	1.22(1)	1.02(0)
16	1.57(1)	9.89(-1)
17	2.01(1)	9.55(-1)
18	2.58(1)	8.73(-1)
19	3.31(1)	8.87(-1)
20	4.26(1)	8.57(-1)
21	5.46(1)	8.25(-1)
22	7.01(1)	7.72(-1)
23	9.01(1)	6.78(-1)
24	1.16(2)	8.35(-1)
25	1.49(2)	8.69(-1)
26	1.91(2)	8.41(-1)
27	2.45(2)	8.02(-1)
28	3.14(2)	7.72(-1)
29	4.04(2)	7.43(-1)
30	5.18(2)	7.01(-1)
31	6.66(2)	6.82(-1)
32	8.55(2)	6.54(-1)
33	1.10(3)	6.25(-1)
34	1.41(3)	6.00(-1)
35	1.81(3)	5.73(-1)
36	2.32(3)	5.48(-1)
37	2.98(3)	5.25(-1)
38	3.83(3)	5.02(-1)
39	4.92(3)	4.81(-1)
40	6.32(3)	4.61(-1)
41	8.11(3)	4.41(-1)
42	1.04(4)	4.22(-1)

*Radial thickness of polyethylene = 0.515 inches: Density of polyethylene = 0.951 gram/cc. Estimated accuracy is ±10% over the entire energy range.

Table V. (Cont'd.)

Group No.	Midpoint Energy (eV)	Response † (counts/incident neut/cm^2)
43	1.34(4)	4.02(-1)
44	1.72(4)	3.84(-1)
45	2.20(4)	3.66(-1)
46	2.83(4)	3.48(-1)
47	3.63(4)	3.30(-1)
48	4.67(4)	3.12(-1)
49	5.99(4)	2.94(-1)
50	7.69(4)	2.76(-1)
51	9.88(4)	2.57(-1)
52	1.17(5)	2.44(-1)
53	1.29(5)	2.36(-1)
54	1.43(5)	2.28(-1)
55	1.58(5)	2.20(-1)
56	1.74(5)	2.11(-1)
57	1.93(5)	2.03(-1)
58	2.13(5)	1.95(-1)
59	2.35(5)	1.86(-1)
60	2.60(5)	1.78(-1)
61	2.88(5)	1.69(-1)
62	3.18(5)	1.61(-1)
63	3.51(5)	1.52(-1)
64	3.88(5)	1.44(-1)
65	4.29(5)	1.36(-1)
66	4.74(5)	1.28(-1)
67	5.24(5)	1.20(-1)
68	5.79(5)	1.12(-1)
69	6.40(5)	1.04(-1)
70	7.07(5)	9.71(-2)
71	7.82(5)	9.01(-2)
72	8.64(5)	8.34(-2)
73	9.54(5)	7.69(-2)
74	1.06(6)	7.08(-2)
75	1.16(6)	6.50(-2)
76	1.29(6)	5.95(-2)
77	1.42(6)	5.44(-2)
78	1.57(6)	4.96(-2)
79	1.74(6)	4.51(-2)
80	1.92(6)	4.09(-2)
81	2.13(6)	3.71(-2)
82	2.35(6)	3.35(-2)
83	2.60(6)	3.01(-2)
84	2.87(6)	2.71(-2)
85	3.17(6)	2.43(-2)
86	3.50(6)	2.18(-2)

Table V (Cont'd.)

Group No.	Midpoint Energy (eV)	Response † (counts/incident neut/cm^2)
87	3.87(6)	1.95(-2)
88	4.28(6)	1.73(-2)
89	4.73(6)	1.53(-2)
90	5.23(6)	1.48(-2)
91	5.78(6)	1.34(-2)
92	6.38(6)	1.19(-2)
93	7.06(6)	9.83(-3)
94	7.80(6)	9.03(-3)
95	8.62(6)	7.95(-3)
96	9.52(6)	7.12(-3)
97	1.05(7)	6.35(-3)
98	1.16(7)	5.57(-3)
99	1.29(7)	4.98(-3)
100	1.42(7)	4.40(-3)

†Interpolation in this table should follow the formula

$$R(E) = R(E_1) \cdot \frac{E_2-E}{E_2-E_1} + R(E_2) \cdot \frac{E-E_1}{E_2-E_1}, \quad \text{for } E_1 \le E \le E_2 .$$

Table VI. Response for 5.88 Inch Diameter Bonner Sphere*

Group No.	Midpoint Energy (eV)	Response † (counts/incident neut/cm²)
1	Thermal	Negligible
2	4.73(-1)	1.89(-1)
3	6.07(-1)	3.38(-1)
4	7.79(-1)	4.45(-1)
5	1.00(0)	5.28(-1)
6	1.29(0)	5.89(-1)
7	1.65(0)	6.36(-1)
8	2.12(0)	6.75(-1)
9	2.72(0)	7.09(-1)
10	3.49(0)	7.39(-1)
11	4.49(0)	7.67(-1)
12	5.76(0)	7.92(-1)
13	7.40(0)	8.17(-1)
14	9.50(0)	8.39(-1)
15	1.22(1)	8.61(-1)
16	1.57(1)	8.81(-1)
17	2.01(1)	8.98(-1)
18	2.58(1)	8.69(-1)
19	3.31(1)	9.31(-1)
20	4.26(1)	9.49(-1)
21	5.46(1)	9.63(-1)
22	7.01(1)	9.51(-1)
23	9.01(1)	8.81(-1)
24	1.16(2)	9.12(-1)
25	1.49(2)	9.99(-1)
26	1.91(2)	1.02(0)
27	2.45(2)	1.02(0)
28	3.14(2)	1.03(0)
29	4.04(2)	1.05(0)
30	5.18(2)	1.04(0)
31	6.66(2)	1.06(0)
32	8.55(2)	1.07(0)
33	1.10(3)	1.07(0)
34	1.41(3)	1.08(0)
35	1.81(3)	1.08(0)
36	2.32(3)	1.09(0)
37	2.98(3)	1.09(0)
38	3.83(3)	1.09(0)
39	4.92(3)	1.10(0)
40	6.32(3)	1.10(0)
41	8.11(3)	1.11(0)
42	1.04(4)	1.11(0)

*Radial thickness of polyethylene = 1.910 inches: density of polyethylene = 0.925 gram/cc. Estimated accuracy is ±10% over the entire energy range.

Table VI (Cont'd.)

Group No.	Midpoint Energy (eV)	Response † (counts/incident neut/cm^2)
43	1.34(4)	1.11(0)
44	1.72(4)	1.12(0)
45	2.20(4)	1.13(0)
46	2.83(4)	1.14(0)
47	3.63(4)	1.15(0)
48	4.67(4)	1.16(0)
49	5.99(4)	1.18(0)
50	7.69(4)	1.20(0)
51	9.08(4)	1.22(0)
52	1.17(5)	1.23(0)
53	1.29(5)	1.24(0)
54	1.43(5)	1.25(0)
55	1.58(5)	1.26(0)
56	1.74(5)	1.27(0)
57	1.93(5)	1.28(0)
58	2.13(5)	1.28(0)
59	2.35(5)	1.29(0)
60	2.60(5)	1.30(0)
61	2.88(5)	1.39(0)
62	3.18(5)	1.31(0)
63	3.51(5)	1.31(0)
64	3.88(5)	1.31(0)
65	4.29(5)	1.31(0)
66	4.74(5)	1.30(0)
67	5.24(5)	1.30(0)
68	5.79(5)	1.29(0)
69	6.40(5)	1.28(0)
70	7.07(5)	1.26(0)
71	7.82(5)	1.25(0)
72	8.64(5)	1.23(0)
73	9.54(5)	1.20(0)
74	1.06(6)	1.18(0)
75	1.16(6)	1.15(0)
76	1.29(6)	1.11(0)
77	1.42(6)	1.08(0)
78	1.57(6)	1.04(0)
79	1.74(6)	9.99(-1)
80	1.92(6)	9.56(-1)
81	2.13(6)	9.06(-1)
82	2.35(6)	8.65(-1)
83	2.60(6)	8.14(-1)
84	2.87(6)	7.55(-1)
85	3.17(6)	7.17(-1)
86	3.50(6)	6.57(-1)

Table VI (Cont'd.)

Group No.	Midpoint Energy (eV)	Response † (counts/incident neut/cm^2)
87	3.87(6)	6.20(-1)
88	4.28(6)	5.84(-1)
89	4.73(6)	5.39(-1)
90	5.23(6)	5.09(-1)
91	5.78(6)	4.81(-1)
92	6.38(6)	4.52(-1)
93	7.06(6)	3.96(-1)
94	7.80(6)	3.69(-1)
95	8.62(6)	3.28(-1)
96	9.52(6)	2.94(-1)
97	1.05(7)	2.62(-1)
98	1.16(7)	2.28(-1)
99	1.29(7)	2.02(-1)
100	1.42(7)	1.80(-1)

†Interpolation in this table should follow the formula:

$$R(E) = R(E_1) \cdot \frac{E_2-E}{E_2-E_1} + R(E_2) \cdot \frac{E-E_1}{E_2-E_1}, \text{ for } E_1 \leq E \leq E_2 .$$

Table VII. Response for 9.86 Inch Diameter Bonner Sphere*

Group No.	Midpoint Energy (eV)	Response † (counts/incident neut/cm^2)
1	Thermal	Negligible
2	4.73(-1)	2.43(-2)
3	6.07(-1)	4.36(-2)
4	7.79(-1)	5.76(-2)
5	1.00(0)	6.85(-2)
6	1.29(0)	7.66(-2)
7	1.65(0)	8.28(-2)
8	2.12(0)	8.81(-2)
9	2.72(0)	9.29(-2)
10	3.49(0)	9.72(-2)
11	4.49(0)	1.01(-1)
12	5.76(0)	1.05(-1)
13	7.40(0)	1.09(-1)
14	9.50(0)	1.13(-1)
15	1.22(1)	1.16(-1)
16	1.57(1)	1.20(-1)
17	2.01(1)	1.23(-1)
18	2.58(1)	1.20(-1)
19	3.31(1)	1.30(-1)
20	4.26(1)	1.34(-1)
21	5.46(1)	1.37(-1)
22	7.01(1)	1.37(-1)
23	9.01(1)	1.28(-1)
24	1.16(2)	1.34(-1)
25	1.49(2)	1.49(-1)
26	1.91(2)	1.53(-1)
27	2.45(2)	1.56(-1)
28	3.14(2)	1.60(-1)
29	4.04(2)	1.64(-1)
30	5.18(2)	1.65(-1)
31	6.66(2)	1.71(-1)
32	8.55(2)	1.75(-1)
33	1.10(3)	1.79(-1)
34	1.41(3)	1.83(-1)
35	1.81(3)	1.86(-1)
36	2.32(3)	1.90(-1)
37	2.98(3)	1.94(-1)
38	3.83(3)	1.98(-1)
39	4.92(3)	2.02(-1)
40	6.32(3)	2.07(-1)
41	8.11(3)	2.12(-1)
42	1.04(4)	2.18(-1)

*Radial Thickness of polyethylene = 4.890 inches: density of polyethylene = 0.951 gram/cc. Estimated accuracy is ±10% for energies above 1 keV and ±25% for energies below 1 keV.

Table VII (Cont'd.)

Group No.	Midpoint Energy (eV)	Response † (counts/incident neut/cm^2)
43	1.34(4)	2.23(-1)
44	1.72(4)	2.30(-1)
45	2.20(4)	2.38(-1)
46	2.83(4)	2.47(-1)
47	3.63(4)	2.57(-1)
48	4.67(4)	2.69(-1)
49	5.99(4)	2.84(-1)
50	7.69(4)	3.03(-1)
51	9.88(4)	3.26(-1)
52	1.17(5)	3.44(-1)
53	1.29(5)	3.57(-1)
54	1.43(5)	3.71(-1)
55	1.58(5)	3.86(-1)
56	1.74(5)	4.02(-1)
57	1.93(5)	4.20(-1)
58	2.13(5)	4.39(-1)
59	2.35(5)	4.61(-1)
60	2.60(5)	4.84(-1)
61	2.88(5)	5.10(-1)
62	3.18(5)	5.35(-1)
63	3.51(5)	5.63(-1)
64	3.88(5)	5.97(-1)
65	4.29(5)	6.29(-1)
66	4.74(5)	6.65(-1)
67	5.24(5)	7.03(-1)
68	5.79(5)	7.42(-1)
69	6.40(5)	7.82(-1)
70	7.07(5)	8.25(-1)
71	7.82(5)	8.68(-1)
72	8.64(5)	9.12(-1)
73	9.54(5)	9.56(-1)
74	1.06(6)	9.98(-1)
75	1.16(6)	1.04(0)
76	1.29(6)	1.08(0)
77	1.42(6)	1.12(0)
78	1.57(6)	1.15(0)
79	1.74(6)	1.18(0)
80	1.92(6)	1.20(0)
81	2.13(6)	1.20(0)
82	2.35(6)	1.22(0)
83	2.60(6)	1.22(0)
84	2.87(6)	1.16(0)
85	3.17(6)	1.19(0)
86	3.50(6)	1.10(0)

Table VII (Cont'd.)

Group No.	Midpoint Energy (eV)	Response † (counts/incident neut/cm^2)
87	3.87(6)	1.11(0)
88	4.28(6)	1.14(0)
89	4.73(6)	1.12(0)
90	5.23(6)	1.10(0)
91	5.78(6)	1.06(0)
92	6.38(6)	1.03(0)
93	7.06(6)	9.81(-1)
94	7.80(6)	9.13(-1)
95	8.62(6)	8.74(-1)
96	9.52(6)	8.05(-1)
97	1.05(7)	7.40(-1)
98	1.16(7)	6.61(-1)
99	1.29(7)	6.05(-1)
100	1.42(7)	5.52(-1)

†Interpolation in this table should follow the formula

$$R(E) = R(E_1) \cdot \frac{E_2 - E}{E_2 - E_1} + R(E_2) \cdot \frac{E - E_1}{E_2 - E_1}, \quad \text{for } E_1 \leq E \leq E_2 \quad .$$

Table VIII. Experimental Configuration for the Iron Slabs

Nominal Iron Thickness (in.)	Actual Iron Thickness (in.)	Detector Locations* Centerline Distance Behind Slab (in.)	Radial Distance from Centerline (in.)	Observation Angle[a] with Respect to ℄ (deg)	Detector Type
1.5	1.55	152	0	0	Bonner Ball
		146	39	15	
		107	107	45	
4	4.05	158	42.5	15	NE-213 Spectrometer
		116	116	45	
6	6.06	162	0	0	NE-213 Spectrometer
12	12.13	141	0	0	Bonner Balls
		136	36.5	15	
		100	100	45	
		156	0	0	NE-213 Spectrometer
		150	40.5	15	
		110	110	45	
	12.25	10	0	0	Benjamin Spectrometer
		10	12	50	
24	24.41	128	0	0	Bonner Balls
		124	33	15	
		90.5	90.5	45	
36	36.56	115	0	0	Bonner Balls
		111	30	15	
		81.5	81.5	45	

*Distances are measured to the geometric center of the Bonner balls, and to the center of detection for the other detectors.

[a]The observation angle is defined as the angle between the centerline and a line connecting the detector with the midpoint of the emergent face of the slab. The vertex of this angle is the pivot point for the angular traverses.

Table IX. Experimental Configurations for the Stainless Steel Slab

Nominal SS Thickness (in.)	Actual SS Thickness (in.)	Detector Locations* Centerline Distance Behind Slab (in.)	Detector Locations* Radial Distance from Centerline (in.)	Detector Locations* Observation Angle[a] with Respect To ℄ (deg)	Detector Type
12	12.17	141	0	0	Bonner Balls
		136	36.5	15	
		100	100	45	
		10	0	0	Benjamin
		10	12	50	Spectrometer

*Distances are measured to the geometric center of the Bonner balls, and to the center of detection for the other detectors.

[a]The observation angle is defined as the angle between the centerline and a line connecting the detector with the midpoint of the emergent face of the slab. The vertex of this angle is the pivot point for the angular traverses.

Table X. Bonner Ball Counting Rates Behind 1.5 in. of Iron (cts/min/watt)

Bonner Ball	3-in.	6-in.	10-in.
On centerline	57.8	607	587
15°	1.02	5.22	4.74
45°	0.680	2.82	1.99

Table XI. Bonner Ball Counting Rates Behind 12 in. of Iron (cts/min/watt)

Bonner Ball	3-in.	6-in.	10-in.
On centerline	2.32	18.5	9.89
15°	0.577	3.54	1.58
45°	0.411	2.39	1.04

Table XII. Bonner Ball Counting Rates Behind 24 in. of Iron (cts/min/watt)

Bonner Ball	3-in.	6-in.	10-in.
On centerline	0.604	3.49	1.40
15°	0.367	1.70	0.600
45°	0.245	1.13	0.405

Table XIII. Bonner Ball Counting Rates Behind 36 in. of Iron (cts/min/watt)

Bonner Ball	3-in.	6-in.	10-in.
On Centerline	0.243	1.08	0.368
15°	0.181	0.700	0.227
45°	0.128	0.475	0.151

Table XIV. Bonner Ball Counting Rates Behind 12 in. of Stainless Steel (cts/min/watt)

Bonner Ball	3-in.	6-in.	10-in.
On Centerline	0.783	5.97	3.51
15°	0.496	2.74	1.28
45°	0.327	1.77	0.797

Table XV. Benjamin Counter Spectrum on the Centerline 10 in. Behind 12 in. of Iron

Energy Interval (keV)	Flux (neuts/cm^2/MeV/min/watt)	Standard Error (%)
	10 Atmosphere Counter	
1379.3-1500	20.4	9.6
1277.1-1379.3	32.3	7.4
1184.2-1277.1	46.4	5.8
1091.3-1184.2	52.4	5.2
1017.0-1091.3	52.4	6.7
933.4-1017.0	65.7	4.6
868.4-933.4	59.2	6.6
803.4-868.4	54.8	6.8
738.4-803.4	91.6	3.9
682.7-738.4	158	2.7
636.2-682.7	195	2.7
589.8-636.2	182	2.9
	3 Atmosphere Counter	
644.7-700	228	3.5
597.9-644.7	233	4.2
551.1-597.9	133	7.0
512.8-551.1	108	10.4
474.5-512.8	118	8.8
436.2-474.5	98.7	9.7
406.4-436.2	129	9.2
372.3-406.4	233	4.1
346.8-372.3	309	4.1
321.3-346.8	351	3.5
295.7-321.3	372	3.1
274.5-295.7	340	4.0
253.2-274.5	254	5.0
236.2-253.2	220	6.8
214.9-236.2	180	6.0

Table XV (Cont'd.)

Energy Interval (keV)	Flux (neuts/cm^2/MeV/min/watt)	Standard Error (%)
	1 Atmosphere Counter	
275.5-300	380	4.0
255.4-275.5	291	6.3
237.5-255.4	215	9.2
219.7-237.5	204	8.9
201.9-219.7	179	9.2
186.2-201.9	273	6.5
172.9-186.2	384	5.1
159.5-172.9	312	5.9
148.3-159.5	334	6.2
137.2-148.3	592	3.3
126.0-137.2	528	3.5
117.1-126.0	317	6.8
108.2-117.1	192	10.3
99.3-108.2	129	14.0
92.6-99.3	156	14.0
85.9-92.6	222	9.1

Table XVI. Benjamin Counter Spectrum 12 in. off the Centerline and 10 in. Behind 12 in. of Iron

Energy Interval (keV)	Flux (neuts/cm^2/MeV/min/watt)	Standard Error (%)
	10 Atmosphere Counter	
1379.3-1500	4.97	12.0
1277.1-1379.3	6.81	10.6
1184.2-1277.1	10.3	7.9
1091.3-1184.2	12.4	6.6
1017.0-1091.3	14.7	7.4
933.4-1017.0	18.6	5.0
868.4-933.4	21.4	5.9
803.4-868.4	20.7	6.0
738.4-803.4	20.7	6.0
738.4-803.4	31.3	3.9
682.7-738.4	52.7	2.8
636.2-682.7	74.8	2.5
589.8-636.2	72.4	2.6
	3 Atmosphere Counter	
645.0-700	69.2	4.4
598.5-645.0	95.8	4.0
552.0-598.5	70.0	5.5
509.7-552.0	54.5	7.6
471.6-509.7	60.8	7.3
437.8-471.6	54.3	8.8
403.9-347.8	51.6	8.6
374.3-403.9	95.4	5.2
344.7-374.3	131	3.6
319.3-344.7	157	3.5
294.0-319.3	167	3.1
272.8-294.0	152	4.1
251.7-272.8	133	4.4
234.7-251.7	120	5.8
217.8-234.7	97.4	6.7

Table XVI (Cont'd.)

Energy Interval (keV)	Flux (neuts/cm^2/MeV/min/watt)	Standard Error (%)
	1 Atmosphere Counter	
275.6-300	165	5.7
255.7-275.6	147	7.8
235.8-255.7	119	9.0
218.1-235.8	107	10.7
202.6-218.1	83.2	14.9
187.1-202.6	130	8.8
173.8-187.1	175	7.3
160.5-173.8	164	7.3
147.2-160.5	159	6.9
136.2-147.2	273	4.6
127.3-136.2	268	5.7
116.2-127.3	189	6.0
107.4-116.2	119	11.0
100.7-107.4	81.3	19.7
91.9-100.7	80.9	13.7
85.2-91.9	113	11.8
78.6-85.2	149	8.4

Table XVII. Benjamin Counter Spectrum on the Centerline 10 in. Behind 12 in. of Stainless Steel

Energy Interval (keV)	Flux (neutrs/cm^2/MeV/min/watt)	Standard Error (%)
	10 Atmosphere Counter	
1379.3-1500	14.0	7.4
1277.1-1379.3	19.6	6.4
1184.2-1277.1	28.2	5.0
1091.3-1184.2	32.4	4.3
1017.0-1091.3	36.2	5.0
933.4-1017.0	41.5	3.7
868.4-933.4	40.6	5.0
803.4-868.4	42.8	4.5
738.4-803.4	61.2	3.0
682.7-738.4	88.1	2.5
636.2-682.7	102	2.6
589.8-636.2	112	2.3
543.3-589.8	101	2.5
506.2-543.3	88.9	3.4
459.8-506.2	90.4	2.5
431.9-459.8	102	3.5
394-431.9	124	2.1
366.9-394.7	145	2.2
339.0-366.9	166	1.9
	3 Atmosphere Counter	
552.3-600	109	6.0
513.4-552.3	87.0	9.3
474.4-513.4	84.7	9.0
439.7-474.4	72.4	11.2
405.1-439.7	83.6	9.0
374.7-405.1	140	5.9
344.4-374.7	166	4.7
318.4-344.4	233	3.8
296.8-318.4	243	4.3

Table XVII (Cont'd)

Energy Interval (keV)	Flux (neuts/cm^2/MeV/min/watt)	Standard Error (%)
275.1-296.8	254	4.0
253.4-275.1	193	5.0
236.1-253.4	163	7.0
218.8-236.1	137	7.7
201.4-218.8	128	7.6
184.1-201.4	153	5.9
171.1-184.1	148	7.4
158.1-171.1	131	7.7
145.1-158.1	223	4.2
	1 Atmosphere Counter	
230.0-250	173	7.4
212.2-230.0	146	9.4
196.7-212.2	120	12.3
181.1-196.7	190	7.2
167.8-181.1	202	7.4
156.7-167.8	168	10.2
143.3-156.7	254	5.1
134.4-143.3	440	4.3
123.3-134.4	412	3.5
114.4-123.3	270	6.2
105.6-114.4	158	9.8
96.7-105.6	136	10.5
90.0-96.7	182	9.5
83.3-90.0	239	6.7

Table XVIII. Benjamin Counter Spectrum 12 in. Off the Centerline and 10 in. Behind 12 in. of Stainless Steel

Energy Interval (keV)	Flux (neuts/cm^2/MeV/min/watt)	Standard Error (%)
	10 Atmosphere Counter	
1380-1500	3.74	14.4
1278.5-1380	5.93	11.1
1186.2-1278.5	7.92	9.3
1093.8-1186.2	10.9	6.9
1010.8-1093.8	13.7	6.3
936.9-1010.8	15.1	6.6
863.1-936.9	16.1	6.1
798.5-863.1	18.4	6.1
743.1-798.5	22.8	5.8
687.7-743.1	36.5	3.6
632.3-687.7	49.4	2.7
586.2-632.3	53.7	3.0
540.0-586.2	50.6	3.2
503.1-540.0	48.1	4.1
466.2-503.1	46.2	4.1
429.2-466.2	49.3	3.7
401.5-429.2	59.8	3.8
364.6-401.5	75.9	2.2
336.9-364.6	89.6	2.4
	3 Atmosphere Counter	
359.4-400	86.8	4.5
338.8-369.4	93.1	4.0
316.9-338.8	133	4.0
290.7-316.9	129	3.3
268.9-290.7	128	3.9
251.4-268.9	102	5.8
229.5-251.4	81.4	5.4
212.0-229.5	75.9	6.8
198.9-212.0	81.5	7.8

Table XVIII (Cont'd.)

Energy Interval (keV)	Flux (neuts/cm^2/MeV/min/watt)	Standard Error (%)
181.4-198.9	93.7	4.8
168.3-181.4	86.5	6.4
155.2-168.3	96.1	5.3
146.4-155.2	162	4.2
	1 Atmosphere Counter	
230.0-250	112	8.1
212.2-230.0	88.9	10.9
196.7-212.2	73.5	14.3
181.1-196.7	100	9.7
167.8-181.1	114	9.4
156.7-167.8	98.7	12.4
143.3-156.7	147	6.3
134.4-143.3	244	5.6
123.3-134.4	240	4.3
114.4-123.3	182	6.7
105.6-114.4	107	10.6
96.7-105.6	70.5	14.7
90.0-96.7	100	12.6
83.3-90.0	150	7.8

Table XIX. NE-213 Spectrum 15 Deg Off the Centerline Behind 4 in. of Iron

	Flux (neuts/cm^2/MeV/min/watt)	
Energy (MeV)	Upper Limit	Lower Limit
0.8	1.11	1.03
0.9	1.04	0.97
1.0	0.98	0.92
1.1	0.92	0.86
1.2	0.82	0.78
1.3	0.74	0.70
1.4	0.68	0.64
1.5	0.65	0.61
1.6	0.62	0.58
1.7	0.57	0.54
1.8	0.52	0.48
1.0	0.48	0.45
2.0	0.46	0.44
2.1	0.46	0.43
2.2	0.45	0.43
2.3	0.44	0.41
2.4	0.43	0.41
2.5	0.41	0.39
2.6	0.40	0.38
2.7	0.37	0.36
2.8	0.345	0.305
3.0	0.285	0.272
3.2	0.235	0.22
3.4	0.20	0.19
3.6	0.185	0.175
3.8	0.185	0.175
4.0	0.185	0.175
4.2	0.177	0.167
4.4	0.158	0.150
4.6	0.140	0.132

Table XIX (Cont'd.)

Energy (MeV)	Flux (neuts/cm^2/MeV/min/watt) Upper Limit	Lower Limit
4.8	0.128	0.120
5.0	0.120	0.113
5.2	0.107	0.100
5.4	0.092	0.085
5.6	0.082	0.076
5.8	0.079	0.073
6.0	0.076	0.070
6.2	0.070	0.064
6.4	0.064	0.059
6.6	0.060	0.0545
6.8	0.0535	0.049
7.0	0.045	0.041
7.2	0.037	0.033
7.4	0.032	0.028
7.6	0.0283	0.0248
7.8	0.026	0.0225
8.0	0.0232	0.020
8.2	0.020	0.0173
8.4	0.0177	0.015
8.6	0.016	0.0133
8.8	0.0144	0.0119
9.0	0.013	0.010
9.2	0.0117	0.0094
9.4	0.0107	0.0086
9.6	0.0100	0.0080
9.8	0.0094	0.0076
10.0	0.0086	0.0069
10.2	0.0077	0.0060
10.4	0.0067	0.0052
10.6	0.0057	0.0043
10.8	0.0046	0.0032
11.0	0.0033	0.0019

Table XX. NE-213 Spectrum 45 Deg Off the Centerline Behind 4 in. of Iron

Energy (MeV)	Flux ($neuts/cm^2/MeV/min/watt$) Upper Limit	Lower Limit
0.8	0.876	0.753
0.9	0.813	0.677
1.0	0.720	0.638
1.1	0.632	0.575
1.2	0.546	0.499
1.3	0.492	0.454
1.4	0.435	0.401
1.5	0.376	0.343
1.6	0.337	0.309
1.7	0.314	0.290
1.8	0.292	0.269
1.9	0.255	0.237
2.0	0.225	0.208
2.1	0.212	0.197
2.2	0.203	0.189
2.3	0.192	0.181
2.4	0.186	0.175
2.5	0.175	0.165
2.6	0.154	0.145
2.7	0.134	0.126
2.8	0.123	0.115
2.9	0.116	0.108
3.0	0.108	0.100
3.2	0.0843	0.0772
3.4	0.0669	0.0596
3.6	0.0580	0.0508
3.8	0.0543	0.0468
4.0	0.0491	0.0421
4.2	0.0480	0.0420
4.4	0.0486	0.0432
4.6	0.0400	0.0350

Table XX (Cont'd.)

	Flux (neuts/cm^2/MeV/min/watt)	
Energy (MeV)	Upper Limit	Lower Limit
4.8	0.0296	0.0252
5.0	0.0252	0.0210
5.2	0.0244	0.0203
5.4	0.0225	0.0189
5.6	0.0190	0.0156
5.8	0.0153	0.0121
6.0	0.0145	0.0114
6.2	0.0140	0.0111
6.4	0.0124	0.00962
6.6	0.0104	0.00780
6.8	0.00931	0.00703
7.0	0.00856	0.00650
7.2	0.00674	0.00464
7.4	0.00564	0.00376
7.6	0.00582	0.00414
7.8	0.00501	0.00334
8.0	0.00312	0.00163
8.2	0.00226	0.00098
8.4	0.00233	0.00109
8.6	0.00223	0.00108
8.8	0.00235	0.00130
9.0	0.00271	0.00172
9.2	0.00256	0.00163
9.4	0.00190	0.00098
9.6	0.00133	0.00052
9.8	0.00113	0.00039
10.0	0.00100	0.00023
10.2	0.00080	0.00005
10.4	0.00075	0.00001
10.6	0.00082	0.00006
10.8	0.00079	0.00006

Table XXI. NE-213 Spectrum on the Centerline Behind 6 in. of Iron

	Flux (neuts/cm^2/MeV/min/watt)	
Energy (MeV)	Upper Limit	Lower Limit
0.8	24.7	22.9
0.9	23.6	21.8
1.0	22.6	21.3
1.1	22.1	21.0
1.2	21.0	20.2
1.3	19.0	18.3
1.4	17.1	16.3
1.5	15.5	14.8
1.6	14.3	13.8
1.7	13.4	12.9
1.8	12.2	11.7
1.9	11.0	10.4
2.0	9.8	9.4
2.1	9.0	8.6
2.2	8.2	7.9
2.3	7.5	7.3
2.4	6.85	6.6
2.5	6.2	6.0
2.6	5.65	5.55
2.7	5.15	5.0
2.8	4.65	4.55
2.9	4.2	4.1
3.0	3.8	3.7
3.2	2.97	2.86
3.4	2.32	2.23
3.6	1.90	1.82
3.8	1.60	1.55
4.0	1.45	1.38
4.2	1.30	1.25
4.4	1.18	1.14
4.6	1.07	1.03

Table XXI (Cont'd.)

	Flux (neuts/cm^2/MeV/min/watt)	
Energy (MeV)	Upper Limit	Lower Limit
4.8	0.945	0.90
5.0	0.82	0.74
5.2	0.68	0.64
5.4	0.605	0.57
5.6	0.56	0.52
5.8	0.52	0.485
6.0	0.49	0.455
6.2	0.44	0.415
6.4	0.39	0.36
6.6	0.345	0.32
6.8	0.325	0.297
7.0	0.300	0.275
7.2	0.268	0.243
7.4	0.222	0.200
7.6	0.190	0.170
7.8	0.175	0.155
8.0	0.165	0.147
8.2	0.154	0.137
8.4	0.143	0.126
8.6	0.134	0.117
8.8	0.124	0.108
9.0	0.113	0.098
9.2	0.104	0.089
9.4	0.095	0.080
9.6	0.084	0.070
9.8	0.071	0.058
10.0	0.060	0.047
10.2	0.050	0.038
10.4	0.042	0.031
10.6	0.039	0.028
10.8	0.041	0.029
11.0	0.044	0.033
11.2	0.046	0.035

Table XXII. NE-213 Spectrum on the Centerline
Behind 12 in. of Iron

	Flux (neuts/cm^2/MeV/min/watt)	
Energy (MeV)	Upper Limit	Lower Limit
0.8	4.8	4.6
0.9	4.2	4.0
1.0	3.9	3.8
1.1	3.65	3.55
1.2	3.35	3.25
1.3	2.7	2.6
1.4	2.1	2.0
1.5	1.65	1.55
1.6	1.35	1.3
1.7	1.12	1.08
1.8	0.94	0.92
1.9	0.78	0.76
2.0	0.66	0.64
2.1	0.54	0.52
2.2	0.46	0.44
2.3	0.38	0.37
2.4	0.315	0.305
2.5	0.255	0.250
2.6	0.210	0.205
2.7	0.170	0.165
2.8	0.143	0.138
2.9	0.119	0.115
3.0	0.097	0.094
3.2	0.068	0.065
3.4	0.050	0.046
3.6	0.037	0.035
3.8	0.030	0.027
4.0	0.027	0.024
4.2	0.0245	0.0220
4.4	0.0205	0.0180
4.6	0.017	0.015
4.8	0.014	0.012

Table XXII (Cont'd.)

Energy (MeV)	Flux (neuts/cm^2/MeV/min/watt) Upper Limit	Lower Limit
5.0	0.0123	0.0105
5.2	0.0117	0.0097
5.4	0.0109	0.0091
5.6	0.0096	0.0080
5.8	0.0080	0.0065
6.0	0.0075	0.0060
6.2	0.0068	0.0052
6.4	0.0063	0.0046
6.6	0.0060	0.0043
6.8	0.0058	0.0042
7.0	0.0054	0.0040
7.2	0.0051	0.0038
7.4	0.0051	0.0037
7.6	0.0050	0.0037
7.8	0.0044	0.0032
8.0	0.0039	0.0028
8.2	0.0038	0.0026
8.4	0.0036	0.0025
8.6	0.0033	0.0022
8.8	0.0027	0.0017
9.0	0.0025	0.0014
9.2	0.0026	0.0016
9.4	0.0028	0.0018
9.6	0.0028	0.0018
9.8	0.0026	0.0016
10.0	0.0023	0.0013
10.2	0.0022	0.0012
10.4	0.0021	0.0013
10.6	0.0021	0.0013
10.8	0.0020	0.0011

Table XXIII. NE-213 Spectrum 15 Deg Off the Centerline Behind 12 in. of Iron

	Flux (neuts/cm^2/MeV/min/watt)	
Energy (MeV)	Upper Limit	Lower Limit
0.8	0.50	0.49
0.9	0.39	0.38
1.0	0.31	0.30
1.1	0.250	0.245
1.2	0.21	0.20
1.3	0.165	0.160
1.4	0.140	0.135
1.5	0.115	0.110
1.6	0.095	0.092
1.7	0.079	0.077
1.8	0.068	0.065
1.9	0.058	0.055
2.0	0.050	0.046
2.1	0.042	0.039
2.2	0.036	0.034
2.3	0.0310	0.0295
2.4	0.0275	0.0255
2.5	0.0240	0.0225
2.6	0.0215	0.0205
2.7	0.0195	0.0180
2.8	0.0175	0.0160
2.9	0.0160	0.0140
3.0	0.0135	0.0120
3.2	0.0088	0.0077
3.4	0.0072	0.0059
3.6	0.0064	0.0054
3.8	0.0061	0.0050
4.0	0.0059	0.0048
4.2	0.0061	0.0051
4.4	0.0056	0.0046
4.6	0.0045	0.0036

Table XXIII (Cont'd.)

Energy (MeV)	Flux (neuts/cm^2/MeV/min/watt) Upper Limit	Lower Limit
4.8	0.0037	0.0028
5.0	0.0032	0.0025
5.2	0.00270	0.00215
5.4	0.00265	0.00195
5.6	0.00265	0.00200
5.8	0.0030	0.0023
6.0	0.0031	0.0024
6.2	0.00260	0.00195
6.4	0.0020	0.0014
6.6	0.0017	0.0011
6.8	0.00160	0.00105
7.0	0.00155	0.00102
7.2	0.00155	0.00100
7.4	0.00148	0.00098
7.6	0.00135	0.00089
7.8	0.00117	0.00076
8.0	0.00108	0.00066
8.2	0.00110	0.00068
8.4	0.00117	0.00076
8.6	0.00120	0.00081
8.8	0.00110	0.00070

Table XXIV. NE-213 Spectrum 45 Deg Off the Centerline Behind 12 in. of Iron

	Flux (neuts/cm^2/MeV/min/watt)	
Energy (MeV)	Upper Limit	Lower Limit
0.8	0.430	0.410
0.9	0.335	0.315
1.0	0.265	0.255
1.1	0.210	0.200
1.2	0.160	0.150
1.3	0.117	0.110
1.4	0.096	0.092
1.5	0.065	0.062
1.6	0.052	0.049
1.7	0.0425	0.040
1.8	0.036	0.034
1.9	0.0290	0.0275
2.0	0.024	0.022
2.1	0.0195	0.0180
2.2	0.0163	0.0148
2.3	0.0140	0.0123
2.4	0.0115	0.0100
2.5	0.0102	0.0092
2.6	0.0087	0.0078
2.7	0.0075	0.0067
2.8	0.0067	0.0057
2.9	0.0056	0.0048
3.0	0.0048	0.0040
3.2	0.0041	0.0033
3.4	0.00355	0.00275
3.6	0.0031	0.0024
3.8	0.00280	0.00215
4.0	0.00245	0.00170
4.2	0.00175	0.00115
4.4	0.00140	0.00080
4.6	0.00160	0.00102

Table XXIV (Cont'd.)

Energy (MeV)	Flux (neuts/cm^2/MeV/min/watt) Upper Limit	Lower Limit
4.8	0.00170	0.00110
5.0	0.00146	0.00090
5.2	0.00124	0.00066
5.4	0.00090	0.00051
5.6	0.00079	0.00034
5.8	0.00071	0.00026
6.0	0.00076	0.00033
6.2	0.00082	0.00039
6.4	0.00068	0.00029
6.6	0.00052	0.00012
6.8	0.00044	0.00006
7.0	0.00048	0.00012
7.2	0.00050	0.00017
7.4	0.00040	0.00011

Table XXV. Approximate Enhancement of the Transmitted Slab Scattered Flux Above Thermal Energy Arising from Multiple Reflection in the Collimator

	ϕ_T Including Collimator/ϕ_T Not Including Collimator
1-1/2 in. of Iron	1.11
12 in. of Iron	1.21
24 in. of Iron	1.21
36 in. of Iron	1.10
12 in. of Stainless Steel	1.17

Table XXVI. Comparison of 220-Group and 100-Group (GAM-II) ANISN Results of Leakage from a 1-Meter-Radius Iron Sphere Arising from a Point Fission Source Located at the Center

ΔE	Groups (220)*	Leakage (220) (neuts/source neut)	Groups (100)*	Leakage (100) (neuts/source neut)	Leakage (220)/Leakage (100)
8-10 MeV	1	5.14(-10)**	5,6,f7	6.79(-10)	0.76
6-8	2	7.13(-10)	f7,8,9,f10	8.42(-10)	0.85
4-6	3,4	1.43(-9)	f10,11-13,f14	1.56(-9)	0.92
3-4	5	3.44(-9)	f14,15,16,f17	3.62(-9)	0.95
2.59-3	6	6.46(-9)	f17,f18	4.10(-9)	1.58
2.231-2.59	7-10,f11	1.20(-8)	f18,19	1.31(-8)	0.92
2.019-2.231	f11	1.32(-8)	20	9.98(-9)	1.32
1.827-2.019	f11,12,13,f14	5.06(-8)	21	2.02(-8)	2.50
1.653-1.827	f14,15-20,f21	1.49(-7)	22	8.25(-8)	1.81
1.496-1.653	f21,22-27,f28	2.64(-7)	23	7.64(-8)	3.46
1.353-1.496	f28,29-35,f36	5.05(-7)	24	2.14(-7)	2.36
1.224-1.353	f36,37-42,f43	1.04(-6)	25	2.72(-7)	3.82
1.108-1.224	f43,44-55,f56	2.01(-5)	26	4.17(-6)	4.82
1.003-1.108	f56,57-63,f64	1.35(-5)	27	3.71(-6)	3.64
0.9072-1.003	f64,65-79,f80	1.42(-4)	28	3.28(-5)	4.33
0.8209-0.9072	f80,81-91,f92	9.37(-5)	29	4.26(-5)	2.20
0.7427-0.8209	f92,93-96,f97	4.55(-5)	30	2.04(-5)	2.23
0.6721-0.7427	f97,98-104,f105	3.67(-4)	31	1.10(-4)	3.34
0.6081-0.6721	f105,106-113,f114	2.62(-3)	32	1.77(-3)	1.48
0.5502-0.6081	f114,115-122,f123	1.95(-3)	33	1.47(-3)	1.33
0.4979-0.5502	f123,124-131,f132	1.16(-3)	34	8.77(-4)	1.32
0.4505-0.4979	f132,133-135,f136	2.22(-3)	35	1.21(-3)	1.83
0.4076-0.4505	f136,137,138,f139	9.84(-4)	36	5.30(-4)	1.86
0.3688-0.4076	f139,140-142,f143	2.86(-3)	37	1.08(-3)	2.65
0.3337-0.3698	f143,144-149,f150	7.86(-3)	38	4.28(-3)	1.84
0.3020-0.3337	f150,151-153,f154	1.48(-2)	39	8.22(-3)	1.80
0.2732-0.3020	f154,155,f156	8.50(-3)	40	4.99(-3)	1.70
0.2237-0.2472	f159,160-162,f163	5.06(-3)	42	3.43(-3)	1.48
0.2024-0.2237	f163,164,165,f166	9.23(-3)	43	5.58(-3)	1.65
0.1832-0.2024	f166,167,f168	5.04(-3)	4	2.43(-3)	2.07
0.1657-0.1832	f168,169-171,f172	1.53(-2)	45	8.99(-3)	1.70
0.1500-0.1657	f172,173,f174	7.07(-3)	46	4.84(-3)	1.46
0.1357-0.1500	f174,175-177,f178	2.05(-2)	47	8.44(-3)	2.43
0.1228-0.1357	f178,179-181,f182	1.27(-2)	48	8.27(-3)	1.54
0.1111-0.1228	f182	7.96(-3)	49	6.40(-3)	1.24
86.52-111.1 keV	f182,183,f184	7.25(-3)	50	5.65(-3)	1.28
67.38-86.52	f184,185-191,f192	2.59(-2)	51	1.48(-2)	1.75
52.48-67.38	f192,f193	7.51(-3)	52	6.20(-3)	1.21
40.87-52.48	f193	4.35(-3)	53	3.78(-3)	1.15
31.83-40.87	f193,f194	2.22(-3)	54	1.76(-3)	1.26
24.79-31.83	f194,195-197,f198	1.94(-2)	55	4.93(-3)	3.94
19.30-24.79	f198,199-201,f202	8.92(-2)	56	8.17(-2)	1.09
15.03-19.30	f202,f203	2.42(-2)	57	2.36(-2)	1.03
11.71-15.03	f203,f204	9.39(-3)	58	1.12(-2)	0.84
9.119-11.71	f204,f205	5.84(-3)	59	4.83(-3)	1.21
7.102-9.119	f205,206,f207	1.21(-3)	60	8.90(-4)	1.36
5.531-7.102	f207,208,f209	1.87(-3)	61	1.92(-3)	0.97
4.307-5.531	f209	3.31(-3)	62	3.51(-3)	0.94
3.700-4.307	f209,f210	1.38(-3)	f63	1.50(-3)	0.87
1.160-3.700	211	8.02(-3)	f63,64-67,f68	7.77(-3)	1.03
0.3167-1.160	212,213	2.01(-3)	f68,69-72,f73	4.33(-3)	0.46
0.0880-0.3167	214	2.98(-3)	f73,74-77,f78	2.96(-3)	1.01
24.4-88.0 eV	215	2.43(-3)	f78,79-82,f83	2.57(-3)	0.95
6.79-24.4	216	1.74(-3)	f83,84-87,f88	1.91(-3)	0.91
1.89-6.79	217	1.01(-3)	f88,89-92,f93	1.14(-3)	0.89
0.524-1.89	218	4.27(-4)	f93,94-98,f99	4.58(-4)	0.93
0.000-0.524	219,220	1.32(-4)	f99,100	5.68(-5)	2.32
Totals	1-220	3.60(-1)	5-100	2.67(-1)	1.35

*Group numbers prefixed with an f lie in more than one energy interval ΔE.

**Read as 5.14×10^{-10}, etc.

ORNL-TM-4222
(ENDF 188)

INTERNAL DISTRIBUTION

1-20. L. S. Abbott
21. C. E. Clifford
22. W. O. Harms
23. R. E. Maerker
24. F. C. Maienschein
25. F. R. Mynatt
26. E. M. Oblow
27. D. B. Trauger
28. D. K. Trubey
29. G. E. Whitesides
30. H. Feshbach (consultant)
31. P. F. Fox (consultant)
32. W. W. Havens (consultant)
33. A. F. Henry (consultant)
34-35. Central Research Library
36-37. ORNL Y-12 Technical Library
Document Reference Section
38-43. Laboratory Records
44. Laboratory Records ORNL RC
45. ORNL Patent Office
46-96. Radiation Shielding Information
Center

EXTERNAL DISTRIBUTION

97-146. Technical Information Center for ENDF distribution
147-148. Technical Information Center
149. Research and Technical Support Division